

Lawrence Berkeley National Laboratory

LBL Publications

Title

Relaxation behavior in low-frequency complex conductivity of sands caused by bacterial growth and biofilm formation by *Shewanella oneidensis* under a high-salinity condition

Permalink

<https://escholarship.org/uc/item/4bd1f86p>

Journal

Geophysics, 86(6)

ISSN

0016-8033

Authors

Joo, Hyun-Woo
Kwon, Tae-Hyuk
Lee, Seung-Rae
et al.

Publication Date

2021-11-01

DOI

10.1190/geo2020-0213.1

Copyright Information

This work is made available under the terms of a Creative Commons Attribution-NonCommercial License, available at <https://creativecommons.org/licenses/by-nc/4.0/>

Peer reviewed

Case History

Relaxation behavior in low-frequency complex conductivity of sands caused by bacterial growth and biofilm formation by *Shewanella oneidensis* under a high-salinity condition

Hyun-Woo Joo¹, Tae-Hyuk Kwon¹, Seung-Rae Lee¹, and Yuxin Wu²

ABSTRACT

Complex electrical conductivity is increasingly used to monitor subsurface processes associated with microbial activities because microbial cells mostly have surface charges and thus electrical double layers. Although highly saline environments are frequently encountered in coastal and marine sediments, there are limited data available on the complex conductivity associated with microbial activities under a high-salinity condition. Therefore, we have developed the spectral responses of complex conductivity of sand associated with bacterial growth and biofilm formation under a highly saline condition of approximately 1% salinity and approximately 2 S/m pore water conductivity with an emphasis on relaxation behavior. A column test is performed, in which the model bacteria *Shewanella oneidensis* MR-1 are stimulated for cell growth and biofilm formation in a sand pack, whereas the complex conductivity is monitored from 0.01 Hz to 10 kHz. The test results indicate

that the real conductivity increases in the early stage due to the microbial metabolites and the increased surface conduction with cell growth but soon begin to decrease because of the reduction of charge passages due to bioclogging. However, the imaginary conductivity significantly increases with time, and clear bell-shaped relaxation behaviors are observed with the peak frequency of 0.1–1 Hz, associated with the double-layer polarization of cells and electrically conductive pili and biofilms. The Cole-Cole relaxation model appears to capture such relaxation behaviors well, and the modeling results indicate gradual increases in normalized chargeability and decreases in relaxation time during bacterial growth and biofilm formation in the highly saline condition. Comparison with previous literature confirms that the high-salinity condition further increases the normalized chargeability, whereas it suppresses the phase shift and thus the imaginary conductivity. Our results suggest that the complex conductivity can effectively capture microbial biomass formation in sands under a highly saline condition.

INTRODUCTION

Microbial growth and activities occur ubiquitously and spontaneously as natural biological processes in the subsurface, or they can be exploited intentionally in engineering practices, such as bioremediation (Zhang et al., 1995), biological soil improvement (Mitchell and Santamarina, 2005; Amos and Ulrich Mayer, 2006; DeJong et al.,

2010; Ham et al., 2018; Kim et al., 2019), and microbial enhanced hydrocarbon recovery (Abdel-Waly, 1999; Park et al., 2017). Geophysical monitoring techniques can provide temporal and spatial information on biological, chemical, mechanical, and hydrologic processes occurring in the subsurface, and they are critical for understanding and successful exploitation of natural or engineered processes, such as microorganism-associated subsurface processes

Manuscript received by the Editor 9 April 2020; revised manuscript received 13 May 2021; published ahead of production 17 August 2021; published online 04 October 2021.

¹Korea Advanced Institute of Science and Technology (KAIST), Civil and Environmental Engineering, Daejeon 34141, Republic of Korea. E-mail: hwj5029@kaist.ac.kr; t.kwon@kaist.ac.kr (corresponding author); srlee@kaist.ac.kr.

²Earth and Environmental Sciences, Lawrence Berkeley National Laboratory (LBNL), Berkeley, California 94720, USA. E-mail: ywu3@lbl.gov.

© 2021 The Authors. Published by the Society of Exploration Geophysicists. All article content, except where otherwise noted (including republished material), is licensed under a Creative Commons Attribution 4.0 Unported License (CC BY-NC). See <http://creativecommons.org/licenses/by/4.0/>. Distribution or reproduction of this work in whole or in part requires full attribution of the original publication, including its digital object identifier (DOI). Commercial reuse is not permitted. The same license does not have to be used for derivative works.

(Abdel Aal et al., 2004, 2010; Atekwana et al., 2004; Williams et al., 2005; Atekwana and Slater, 2009; Davis et al., 2010; Karaoulis et al., 2011; Kwon and Ajo-Franklin, 2013; Noh et al., 2016).

Among various geophysical properties, microbial activities have a pronounced effect on electrical responses in porous media, including surface conduction, because bacterial cells are known to have surface charges and thus an electrical double layer (Fröhlich, 1975; Foster and Schwan, 1986; Atekwana and Slater, 2009). Therefore, the spectral-induced polarization (SIP) method, also known as the complex electrical conductivity method, has been widely used in biogeophysical monitoring studies; and the SIP has demonstrated its capability of monitoring various microbial activity, such as microbial growth, cell adsorption in minerals, biofilm and biopolymer formation, bioclogging, changes in electrolyte properties, and even the inactivity of some microbial cells (Abdel Aal et al., 2004, 2009; Ntarlagiannis et al., 2005; Davis et al., 2006, 2010; Atekwana and Slater, 2009; Ntarlagiannis and Ferguson, 2009; Wu et al., 2014). Specifically, it is reported that the imaginary conductivity, which captures polarization, increases with bacterial cell density and biofilm formation in electrically inactive, clean quartz sands (Abdel Aal et al., 2004, 2010; Davis et al., 2006; Zhang et al., 2013, 2014; Mellage et al., 2018, 2019). The relevant polarization and relaxation behavior in association with bacterial cells has been identified and modeled using the Cole-Cole relaxation model (Revil et al., 2012; Mellage et al., 2018, 2019). These previous studies advance our understanding of the SIP responses associated with microbial growth and biofilm formation; most of studies are limited

to low-salinity conditions with electrical conductivity of less than 1 S/m. But we often encounter high-salinity environments with salinity greater than 1% and electrical conductivity greater than 2 S/m, including coastal and marine sediments and deep hydrocarbon reservoirs (Weller et al., 2015; Kimak et al., 2019; Wu and Peruzzo, 2020). Nevertheless, experimental evidence of the relaxation behavior associated with microbial growth and biofilm formation under a high salinity condition is still scarce, including their effects on the normalized chargeability and relaxation time.

This study presents the low-frequency SIP response and relaxation behavior of the complex conductivity of sands associated with microbial growth and biofilm formation under a high-salinity condition. Column experiments were performed, in which the model bacterium *Shewanella oneidensis* MR-1 was cultured and stimulated for biofilm formation in a sand pack, whereas the SIP responses were monitored at low frequencies (0.01–10,000 Hz). The *S. oneidensis* MR-1 (ATCC# 700550) was selected as the model microorganism because of its metal-reducing capability, which is beneficial in bioremediation practices (Xiong et al., 2006; Icopini et al., 2009; Lee et al., 2018), and for its biofilm-forming capability, which causes problematic bioclogging in wastewater treatment (Engel et al., 2019). Furthermore, the spectral responses associated with microbial growth and biofilm formation are analyzed using the Cole-Cole relaxation model, and the variations in normalized chargeability and relaxation time are discussed in relation to changes in cell density and microbially produced organic compounds.

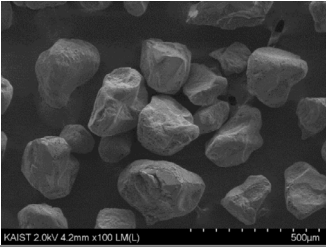
MATERIALS AND METHODS

Host sand, model bacteria, and defined growth media used

Fine silica sand (Ottawa F110, U.S. Silica, Frederick, Maryland, USA) was used as the host sand (see Table 1). Ottawa F110 sand was sieved with a no. 200 sieve to remove fine particles, and the sieved sand was then washed with 70% ethanol and rinsed with deionized water to remove organic contaminants. The rinsed sand was sterilized in an autoclave at 121°C for 20 min and then oven dried at 110°C for more than 24 h prior to being packed in a column.

In this study, *S. oneidensis* MR-1 (ATCC# 700550) was selected as the model microorganism. *Shewanella* spp. are commonly found in soil and aquatic environments, and *S. oneidensis* MR-1 is a gram-negative bacterium known for its ability to thrive in anaerobic and aerobic environments. The model bacteria *S. oneidensis* MR-1 have been intensively studied for their ability to reduce metals, such as iron, plutonium, mercury, and uranium (Xiong et al., 2006; Icopini et al., 2009; Lee et al., 2018). In addition, *S. oneidensis* MR-1 is well known for its unique and interesting capability to produce electrically conductive nanowires and biofilms, which assist in the transport of electrons and nutrients, facilitating survival in harsh environments, as shown in Figure 1 (Gorby et al., 2006; Roy et al., 2013). In this

Table 1. Physical properties and test conditions of the experiment.

Parameter	Value
Scanning electron microscopy (SEM) image of host sand	
Host porous medium (sand pack)	
Mean grain diameter	$D_{50} = 143 \mu\text{m}$
Effective grain diameter	$D_{10} = 87 \mu\text{m}$
Particle shape	Roundness = 0.7 ³ , Sphericity = 0.7 ³
Porosity	0.355
Fresh growth media	
Pore water conductivity	2.175 S/m
pH	6.8
Flow rate	1 mL/min
Flow condition	
Seepage velocity	3.57 mm/min
Duration	469 h
Temperature	28 ± 1°C

Note: ³Cho et al. (2006) and Cortes et al. (2009).

study, we also confirmed the production of pili and biofilms by the model bacteria (Figure 1).

Tryptic soy broth (TSB) diluted four times with additional sodium chloride (7 g/L of NaCl) and 0.1 M potassium phosphate buffer solution (PBS) was used as the growth medium to culture model bacteria. The chemical composition of the defined growth medium is summarized in Table 2. Although microbial metabolites can change the ionic strength in the pore fluid and thus the bulk electrical conductivity, NaCl salt was intentionally added to increase the pore water salinity so as to minimize the effect of microbial metabolites on the electrical conductivity of the pore fluid. The growth medium contained the PBS to provide a consistent pH condition for bacterial growth and activity. The pH and salinity of the fresh growth media used in this study were approximately 6.8 and 1.2%, respectively. Accordingly, the electrical conductivity was approximately 2.2 S/m, which is mostly higher than that of the previous studies (e.g., approximately 0.1 S/m in Abdel Aal et al. [2010], less than 0.5 S/m in Revil et al. [2012], 0.025 S/m in Zhang et al. [2014], and approximately 0.1 S/m in Rosier et al. [2019]). Therefore, our growth medium represents a high-salinity condition that is often found in coastal and marine environments and in deep hydrocarbon reservoirs. Prior to the column experiment, a frozen culture of *S. oneidensis* MR-1 was resuscitated and aerobically cultured in a 200 mL growth medium at 30°C without shaking. This initial culture was transferred twice to the fresh growth medium (1:10 v/v); thereafter, the 200 mL freshly grown culture was transferred to the 2000 mL fresh growth medium. This was used as the inoculum to be injected to the sand pack column. The cell concentration of the inoculum was estimated to be approximately 2×10^8 cells/mL. The doubling time for cell growth kinetics was estimated to be 4.5 h. More details about the growth kinetics, optical density, and cell density of the model bacteria as well as the electrical conductivity of the liquid culture can be found in the supplemental information that can be accessed through the following link: Figure S1.

Column setup

A cylindrical polycarbonate column with a length of 308 mm and an inner diameter of 31 mm was used as the bioreaction column containing the host sand (Figure 2). All fittings and top and bottom caps, made of polytetrafluoroethylene, were compatible with autoclave sterilization and electrical conductivity measurements, preventing electric current leakage. A high-pressure liquid metering pump (OPTOS 2SMP, Eldex Laboratories, Inc., California, USA) provided continuous feeds of the inoculum and subsequently the fresh growth medium at a controlled flow rate. One backpressure regulator was installed to apply backpressure of 300 kPa to minimize the nucleation of biogenic gas bubbles and maintain a fully water-saturated condition. The column experiment was conducted at a constant temperature of 28°C in a temperature-controlled incubator, minimizing the effect of temperature on complex electric conductivity measurements.

Complex electrical conductivity measurement

Two silver-silver chloride (Ag-AgCl) coiled electrodes were placed at both end caps and were used as the current electrodes to supply electric current to the water-saturated sand pack (Figure 2). Four Ag-AgCl potential electrodes were inserted from the side of the column with regular spacing of 65 mm to measure the electrical potential drops between them. These potential electrodes were named in a numerical order from the inlet to the outlet, e.g., electrodes 1–4. Each potential electrode was housed in a tube filled with pore fluid and without agar protection, such that the potential electrodes were electrically in contact with the pore fluid but did not come into direct contact with the sand grains to avoid spurious polarization errors (Ulrich and Slater, 2004). Because the electrodes are regularly spaced, the entire column can be divided into three subsections (sections 1–3 from the inlet to the outlet). Therefore, the electrical potential drops and the phase shifts between electrodes 1 and 2, 2 and 3, 3 and 4, and 1 and 4 represent the responses of the corresponding sections. The potential and phase shift measurements were conducted using a multi-function data acquisition system (DAQ; PXIe-6356, National Instrument, Texas, USA). Five cycles of continuous sinusoidal waves were supplied to two current electrodes at 1.0 Vpp, whereas the electrical potential differences between the electrodes were acquired at the sampling rate of 1.25 MS/s (Nyquist frequency of 625 kHz). The frequency of the imposed sinusoidal waves was controlled to sweep from 10^{-2} to 10^4 Hz with logarithmically increasing intervals, and each measurement was repeated five times for averaging. The operational

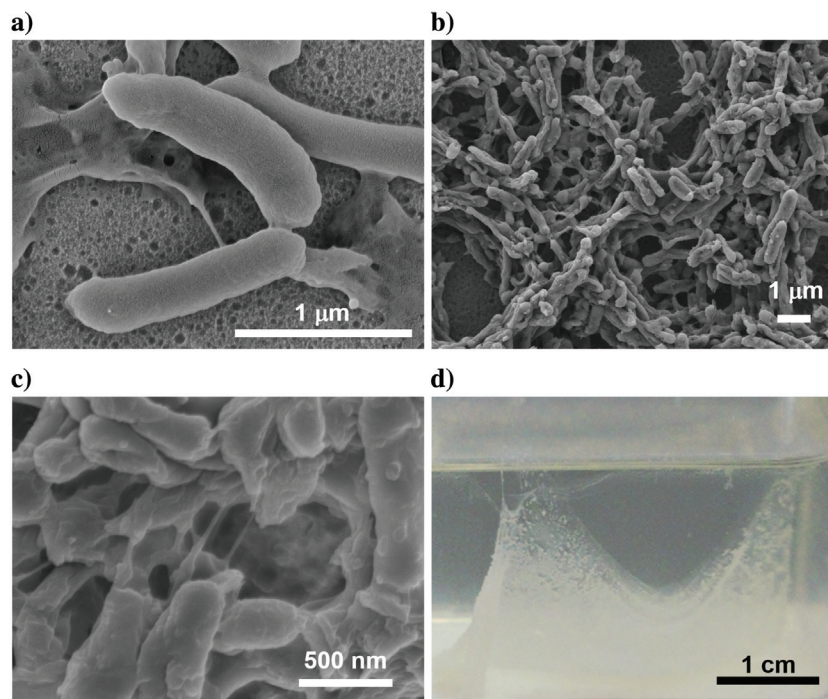


Figure 1. Bacterial cells and biofilms of *S. oneidensis* MR-1. The SEM image of (a) bacterial cells, (b) bacterial colonies, and (c) bacterial cells interconnected with pili and nanowires. The bacterial cells and biofilms cultured on a glass plate and their samples for SEM imaging were prepared by following the cell fixation and dehydration processes suggested by Cen et al. (2004). (d) A digital image of biofilms formed in an aerobic culture of *S. oneidensis* MR-1. The bacteria cultures were aerobically grown in separate batches, in which their inoculums were collected from the effluent samples and transferred to fresh growth media.

amplifiers (i.e., made of AD620, Analog Devices, Massachusetts, USA) were used to increase the input DAQ impedance to $10^{10} \Omega$, minimizing current leakage, and to amplify and regulate the electrical potential signals (Slater et al., 2005). Accordingly, the impedance

magnitude ($|Z|$) and the phase angle (ϕ) were measured from 0.01 Hz to 10 kHz. Hence, the real and imaginary conductivities are computed from the measured values by using the geometric factor (G) as follows:

$$\sigma' = \frac{G}{|Z|} \cdot \cos \phi = \frac{L/A}{|Z|} \cdot \cos \phi, \quad (1)$$

and

$$\sigma'' = \frac{G}{|Z|} \cdot \sin \phi = \frac{L/A}{|Z|} \cdot \sin \phi, \quad (2)$$

where Z and ϕ are the impedance and phase angle, respectively, L is the distance between the measuring potential electrodes, and A is the cross-sectional area of the sand pack column; these two values are given by the configuration of the column and electrode setup. The term G is the geometric factor, which can be obtained from the calibration. In an ideal case, in which the electric current flux is parallel, the geometric factor becomes identical to the distance divided by the area, i.e., $G = L/A$.

Calibration of the measurement system was carried out using sodium chloride (NaCl) solutions with various concentrations (0.05, 0.25, 0.50, 0.80, 1.00, and 2.00 M). Note that previous studies have suggested that reliable measurements can be made with phase angles of less than 0.1 mrad below 100 Hz (Zimmermann et al., 2008; Revil and Skold, 2011; Zhang et al., 2014). For the tested calibration solutions with an NaCl concentration greater than 0.25 M, our measurement system showed phase angle values of less than 0.013 mrad below 10 Hz and less than 0.05 mrad below 100 Hz (supplemental information can be accessed through the following link: Figure S2), allowing reliable and consistent measurement of the complex conductivity. Based on this calibration, the geometric factor G was computed to be 250.7 m^{-1} , which is fairly close to the L/A value of 247.5 m^{-1} , with less than a 1.3% difference.

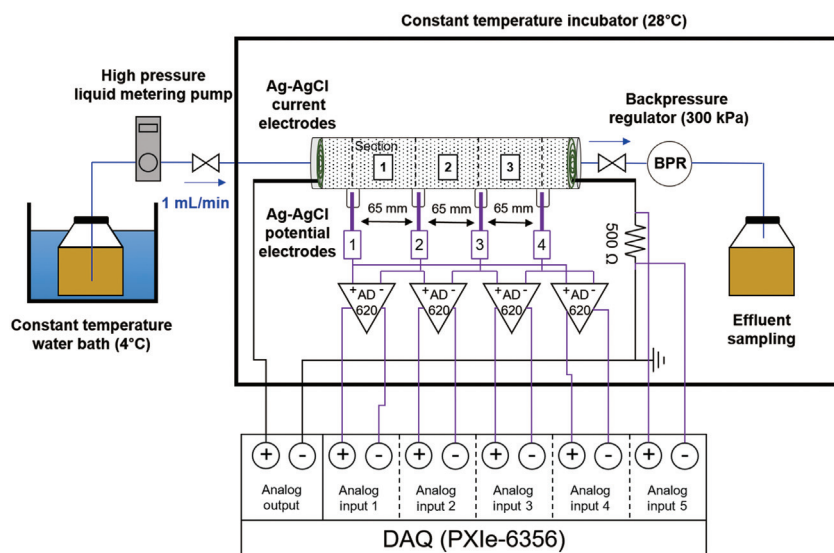


Figure 2. The schematic diagram of the experimental setup. The blue and black lines indicate fluid and electrical current flow, respectively, whereas the purple lines show potential measurement.

Table 2. Chemical composition of 25% diluted TSB medium.

Compound	Concentration
Casein peptone	4.25 g/L
Soya peptone	0.75 g/L
Glucose	0.625 g/L
K_2HPO_4	0.625 g/L
NaCl	7 g/L
Phosphate buffer (pH = 6.8)	0.1 M

Table 3. Estimated Cole-Cole model parameters.

Parameter	Elapsed time (h)			
	4	37	133	469
σ' at high frequency σ'_{∞} (S/m)	0.5952	0.6374	0.5809	0.5647
σ' at low frequency σ'_0 (S/m)	0.5992	0.6672	0.6536	0.6758
Chargeability M	0.0068	0.0467	0.1251	0.1966
Normalized chargeability M_n (S/m)	0.004	0.0298	0.0726	0.111
Relaxation time τ (s)	0.94	0.41	0.2	0.16
Cole-Cole parameter c	0.79	0.9	0.8	0.79
Note	4 h elapsed since inoculation	Fresh nutrient feed commenced	Glucose concentration converged	Nutrient injection terminated

Column preparation and experiment procedure

The sand pack was prepared by wet pluviating and hand tamping the sterilized dry sand in the fresh growth medium. The initial porosity of the sand pack was 0.355, and the initial permeability was measured to be $1 - 2 \times 10^{-12} \text{ m}^2$ (or 1–2 darcy). The pore volume (PV) of the sand pack column was approximately 78.3 mL. The sand pack column was flushed with the fresh growth medium at a flow rate of 1 mL/min for 6 h, equivalent to approximately 4.6 times the PV. Thereafter, the sand pack was inoculated with the *S. oneidensis* MR-1 culture at 1 mL/min, and 2200 mL of inoculum was injected, which is approximately 28 PV. This point when we commenced the cell inoculation was defined as the starting point, i.e., 0 h. After cell inoculation for 36.7 h (approximately 1.5 days), the injection of fresh growth media then continued at 1 mL/min for 432.3 h (approximately 18 days) to stimulate bacterial growth and biofilm formation (i.e., continuous nutrient injection). Thereby, the flow duration was 469 h (approximately 19.5 days) in total. The complex conductivity was monitored every 3 h. Owing to the motility of *S. oneidensis* MR-1, the bacteria can grow in the fresh growth media prior to being injected into the sand pack. To prevent bacteria from growing in the media bottle but to limit the growth only in the sand pack inside, the liquid growth media to be injected were stored at 4°C in a temperature-controlled bath during the entire experiment (Figure 2). The temperature of the sand pack column, where the bacterial growth and biofilm formation were stimulated, was maintained at $28.0 \pm 1.0 \text{ }^\circ\text{C}$ during the experiment. Table 1 summarizes the experimental condition. For comparison, an abiotic control test was performed for 230 h (approximately 9.6 days) without bacterial inoculation, whereas the other conditions were kept the same. The results can be found in the supplemental information that can be accessed through the following link: Figure S3.

Influent/effluent analysis and postexperiment scanning electron microscopy

During continuous nutrient injection, approximately 55 mL of influent and approximately 55 mL of effluent were collected every 24 h. Immediately after sampling, the optical density at a wavelength of 600 nm (OD_{600}), glucose concentration, pH, and pore water conductivity (σ_w) of those influent and effluent samples were measured daily to obtain the pore fluid characteristics and confirm the bacterial growth. In addition, the cell density in the effluent was estimated from the optical density through the calibration using quantitative polymerase chain reaction analysis (see the supplemental information that can be accessed through the following link: Figure S1). The glucose concentration was obtained using high-performance liquid chromatography (HPLC) (1260 infinity HPLC, Agilent Technologies, California, USA). All of the measurements were repeated three times and averaged. In addition, the effluent samples collected every two days were

analyzed using the 16S ribosomal RNA (16S rRNA) genetic sequence method to confirm the purity of the cultured bacteria in the effluent stream. Upon completion of the column experiment that lasted 469 h, the wet sand samples containing bacterial cells and biofilms were collected, air dried for 2–3 h, and then imaged using environmental scanning electron microscopy (ESEM; FEI Quanta 650 FEG) without any coating.

RESULTS

Variations in cell density, glucose concentration, pH, and electrical conductivity

Changes in the cell density, glucose concentration, and pH of the effluent confirmed the bacterial activity in the sand pack column, as shown in Figure 3. The cell density increased because of the bacterial cell growth for the first 72 h (three days). Then, it continued to increase and range approximately $3.5\text{--}6.5 \times 10^9$ cells per mL. However, there was some fluctuation possibly because of the optical interference effect of biofilms and the variation in microbial growth (Figure 3a). Overall, it is presumed that the planktonic cell density

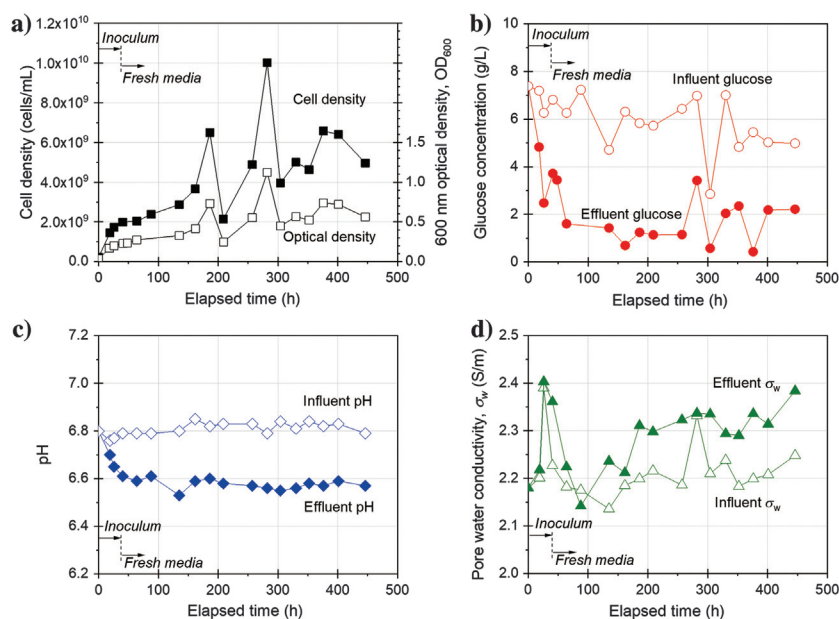


Figure 3. Influent and effluent analysis results. (a) Cell density and 600 nm optical density of effluent, (b) glucose concentration, (c) pH, and (d) pore water conductivity.

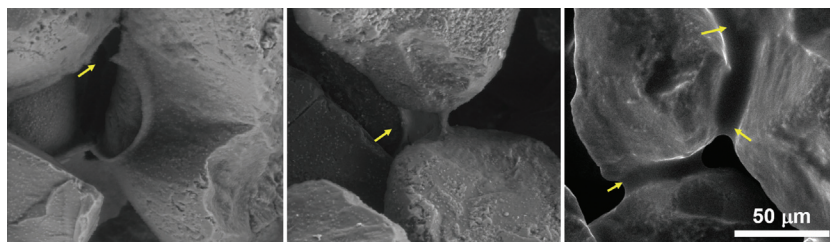


Figure 4. ESEM images of sand grains after the column experiment. The yellow arrows indicate biofilms between the F110 particles.

in pores increased during the first 72 h and, thereafter, was kept constant. Meanwhile, the detached biofilms were consistently observed in the effluent after 72 h, which primarily caused the continued

increase in OD_{600} with some variability. Similar to the cell density trend, the glucose concentration decreased during the first 72 h because of highly activated bacterial metabolisms during the cell growth.

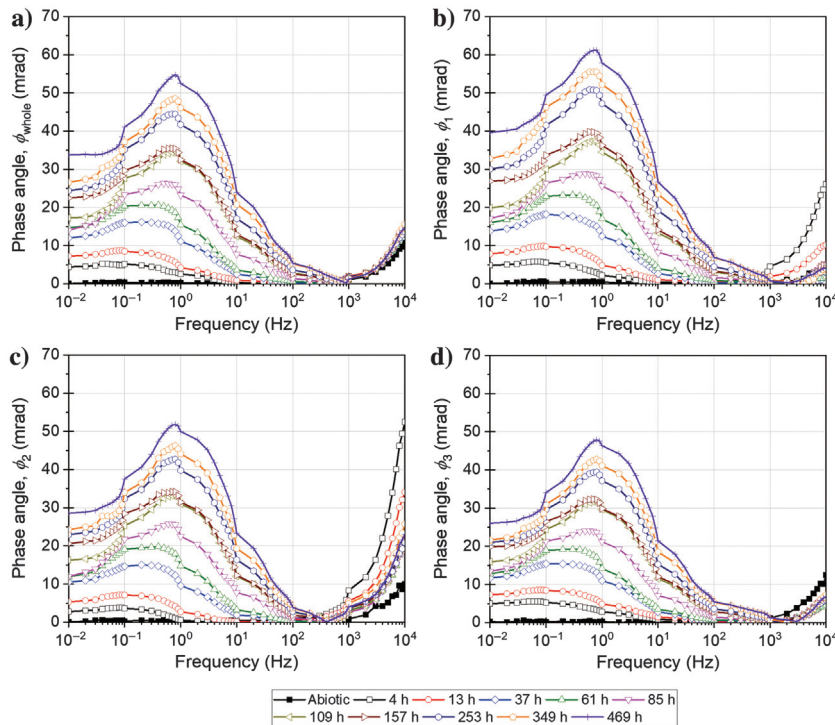


Figure 5. Spectral responses of the phase angle: (a) the whole section, (b) section 1, (c) section 2, and (d) section 3.

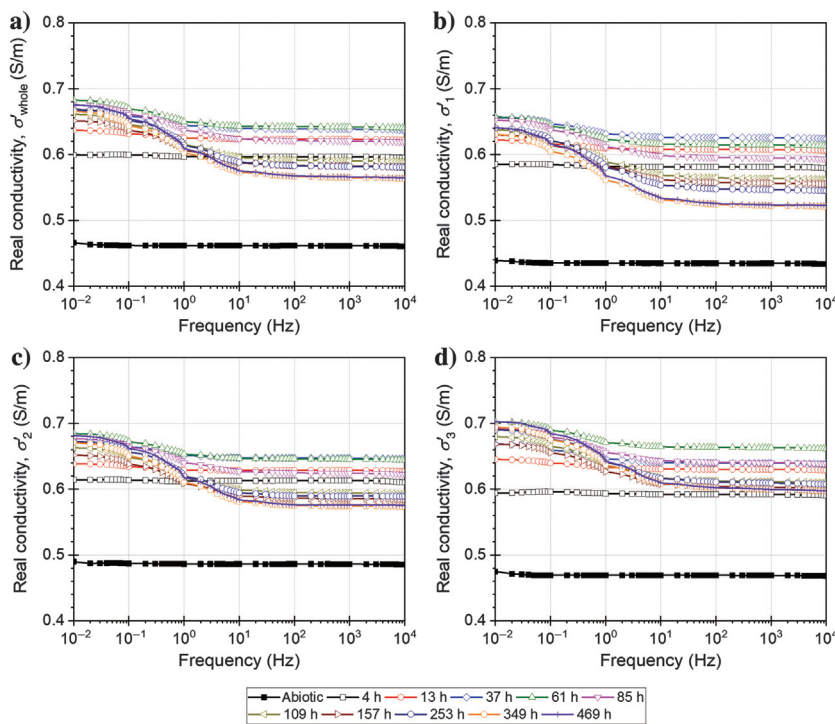


Figure 6. Spectral responses of real conductivity: (a) the whole section, (b) section 1, (c) section 2, and (d) section 3.

Thereafter, the glucose concentration in the effluent was leveled off, but not completely consumed (Figure 3b). This indicates that the nutrient feed was sufficient for microbial population in the column to keep their metabolite and microbial activities i.e., a nutrient-rich condition. Note that 1.3 h takes for 1 PV injection (the flow rate was 1 mL/min and the PV is 78.3 mL) and that the doubling time is approximately 4.5 h. This nutrient-rich condition also facilitated spatially consistent SIP responses along the column, as shown later in this paper. ESEM imaging after the experiment also confirmed the bacterial growth and biofilm formation on sand grains (Figure 4).

The bacterial growth and their metabolites decreased the pH value from 6.8 to approximately 6.6 during the first 72 h; thereafter, the pH value was maintained consistently at approximately 6.5–6.6 owing to the phosphate buffer in the fresh growth medium that was continuously supplied (Figure 3c). The high salinity of our growth medium caused only a slight increase in the pore water conductivity (σ_w) of pore fluids, from 2.2 to approximately 2.4 S/m (Figure 3d).

Responses of complex electrical conductivity

Figures 5, 6, and 7 show the spectral responses in the phase angle and complex conductivity (phase angle ϕ , real conductivity σ' , and imaginary conductivity σ'') at a frequency range from 10^{-2} to 10^4 Hz over the course of the column experiment, which lasted approximately 469 h. Installation of four potential electrodes enables the electrical measurement on three sections (i.e., ϕ_1 , ϕ_2 , ϕ_3 , σ_1^* , σ_2^* , and σ_3^* for sections 1, 2, and 3, respectively) as well as for the entire length between the two electrodes at the very ends (or the whole section; i.e., ϕ_{whole} and σ_{whole}^* from electrodes 1 and 4). The phase angle of the whole section before cell inoculation was initially less than 1 mrad (indicated as *abiotic*), but it soon increased to approximately 5 mrad at $f = 0.1$ Hz 4 h after the commencement of cell inoculation. The phase angle continued to increase up to greater than 20 mrad for $f = 0.01$ –10 Hz. Among the sections, the closer to the inlet, the higher the phase angle that was found (Figure 5).

Spectral responses of real conductivity

In the beginning, σ' initially ranged approximately 0.58–0.62 S/m at 4 h, as shown in Figure 6. In all sections, the initial σ' values were primarily

determined by the pore water conductivity (σ_w) and porosity; these were in a similar range, implying fairly homogeneous sample preparation (Figure 6). In the beginning at 4 h, σ' showed no or minimal frequency-dependent behavior. Soon, bacterial cell growth and biofilm formation with continued nutrient injection caused the gradual manifestation of the relaxation response of the real conductivity σ' in all sections (σ'_1 , σ'_2 , σ'_3 , and σ'_{whole}), where σ' decreased with an increase in frequency at the relaxation frequency of approximately 0.1–1.0 Hz. Moreover, the σ' difference at $f = 0.01$ Hz and σ' at $f = 10^4$ Hz gradually increased with time.

Figure 8a and 8b shows the temporal variations in σ' at various frequencies and in different sections. The early increase in σ' up to approximately 72 h was attributable to the microbial metabolites from metabolic activity and the increased surface conduction with cell growth and attachment. Noting that the electrical conductivity of the effluent stayed in a narrow and consistent range of 2.2–2.4 S/m (Figure 3d), the surface conduction by cell attachment on the grain surfaces played a more significant role in such an early increase in σ' compared to the fluid conductivity rise by the microbial metabolites. After 72 h, as bacteria began to produce biofilms, the accumulation of biofilms reduced charge passages in the sand pack and contributed to overall decreases in σ' , although the reduction in the pore space is expected to be fairly small. Therefore, the reduction in σ' was limited to less than 15%, from approximately 0.65 to 0.57–0.61 S/m at $f = 1$ –100 Hz. Such σ' reductions are more prominent in the frequency regime higher than the relaxation frequency (i.e., $f >$ approximately 1 Hz; Figure 8a), consistently observed in all sections across the entire column (Figure 8b).

Spectral responses of imaginary conductivity

The spectral responses of the imaginary conductivity σ'' are shown in Figure 7, similar to the phase angle trends. The initial spectral response of σ'' at 4 h in the low-frequency regime was mostly attributed to the planktonic bacterial cells inoculated and suspended in the pore fluid prior to the initial attachment phase. Thereafter, bacterial cell growth and biofilm formation, which are electrically polarizable, caused an overall increase in σ'' with continued nutrient injection in all sections (Figure 7). Similar to σ' , the spectral responses of σ'' also revealed a distinct relaxation response with the relaxation frequency at approximately 0.1–1.0 Hz, and such relaxation responses became more prominent with time. Again, the measured σ'' changes were consistent in all sections, with little variation with location. For comparison, we ran an abiotic control test that lasted 230 h,

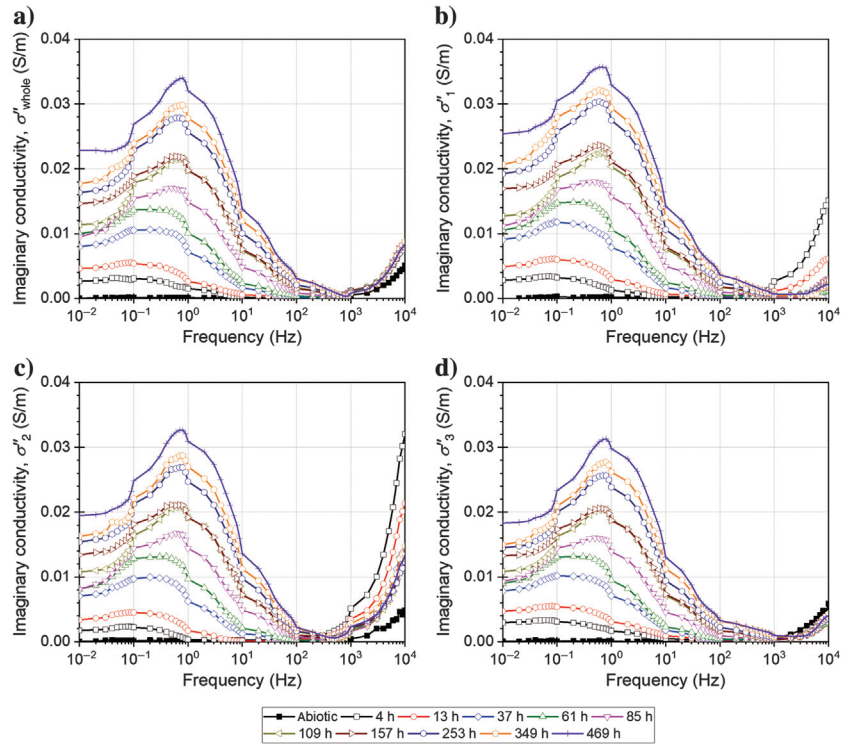


Figure 7. Spectral responses of imaginary conductivity: (a) the whole section, (b) section 1, (c) section 2, and (d) section 3.

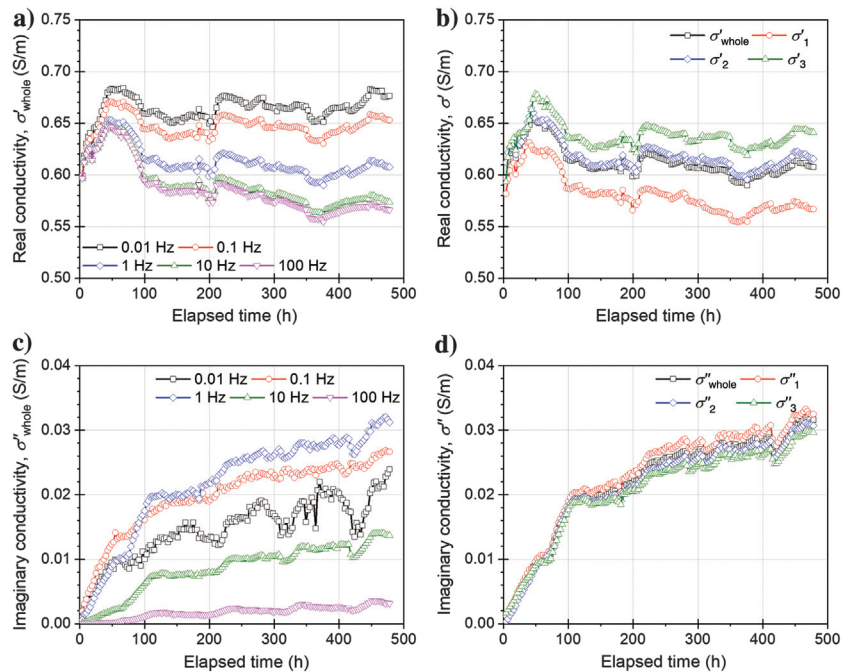


Figure 8. Variations in complex conductivity with time: (a) real conductivity at $f = 0.01$, 0.1, 1, 10, and 100 Hz for the whole section, (b) real conductivity at 1 Hz for each section, (c) imaginary conductivity at $f = 0.01$, 0.1, 1, 10, and 100 Hz for the whole section, and (d) imaginary conductivity at 1 Hz for each section.

in which the same testing condition, such as growth medium composition, host sand pack, and flow rate, was applied while only excluding the inoculation of bacteria. During the abiotic control run, there was no or only minimal change in the spectral responses of σ'' and the σ'' values were kept less than 5×10^{-3} S/m with the phase angle less than 1 mrad (see the supplemental information that can be accessed through the following link: Figure S3).

Figure 8c and 8d shows the temporal variations in σ'' at various frequencies and different sections. At frequencies of less than 1 kHz, σ'' significantly increased with continued bacterial activity and biomass accumulation, although their extent differs with frequency. The greatest increase was found at $f = 1$ Hz, and the smallest change corresponded to $f = 100$ Hz, owing to the relaxation behavior.

The real conductivity σ' is primarily determined by the amount of the movable charges in pore fluids and the charge passage in porous media. Because the growth medium composition is maintained consistent, the variations in the salinity of the influent and effluent are minimal. Hence, the observed σ' reduction in the sand pack is attributable to the accumulation of biomass in the pores, which reduces the charge passage. In contrast, the imaginary conductivity σ'' is heavily affected by the polarizability of the materials produced by bacteria, which includes cells and extracellular polymeric substances (EPS). The observed significant rises in σ'' can be explained by the accumulation of electrically polarizable bacterial cells and biofilms because the model bacteria *S. oneidensis* MR-1 are well known to produce biofilms. This rise in the imaginary conductivity σ'' associated with bacterial growth and activity has been consistently reported in previous studies that were mostly carried out under a low-salinity condition with pore water conductivity of less than 0.5 S/m (e.g., Ntarlagiannis et al., 2005; Davis et al., 2006, 2010; Abdel Aal et al., 2009, 2010; Ntarlagiannis and Ferguson, 2009; Mellage et al., 2018). However, our result provides clear confirmation that the bacterial growth and biofilm growth can increase the imaginary conductivity σ'' even in a high-salinity condition (approximately 1.2%) with the pore water conductivity greater than 2 S/m, which is a previously unexplored salinity range. Interestingly, the relaxation time appears to decrease with time (opposite in peak frequency in Figure 7). This decrease in the relaxation time is presumed to be attributable to the major changes in the biomass composition. This will be further discussed in the “Analysis and discussion” section.

To ensure the reliability and repeatability of the observed results, we provide additional data obtained from a preliminary test that was carried out before the main column test (see the supplemental information that can be accessed through the following link: Table S1 and Figure S4). The test condition in this preliminary run, such as the host soil, model bacteria, and test procedure, was mostly the same with that of the main test, but the growth medium without the pH buffer was injected at a lower fluid injection rate (0.5 mL/min). Thereby, the absence of buffer caused a gradual reduction in pore fluid pH and retarded the bacterial growth and EPS production. This is supported by the low OD₆₀₀ values of the effluent samples compared to those in the main test. As a result, the increment in the imaginary conductivity in this preliminary test was lower than that in the main test. However, the general tendency was consistent with the main test results — significant increases in σ'' during cell growth and biofilm formation by *S. oneidensis*, although the extent differs with the location owing to the low pH, low cell density, and slower nutrient feed (see the

supplemental information that can be accessed through the following link: Figure S4).

ANALYSIS AND DISCUSSION

The α -polarization associated with bacterial biomasses

Negatively charged surfaces of bacterial cells, similar to clay particles, can exhibit three polarization modes: α -, β -, and γ -polarizations (Fröhlich, 1975; Foster and Schwan, 1986; Atekwana and Slater, 2009; Revil et al., 2012). At low frequencies of less than 100 Hz ($f < 100$ Hz), double layers around negatively charged cells and/or bacterial organic materials can be polarized, referred to as α -polarization (Grosse, 2002). In the kilo- to megahertz frequency range ($f = 10^3$ – 10^6 Hz), the interfacial polarization due to ion accumulation in the cytoplasm of a bacterial cell can be developed, referred to as β -polarization (or Maxwell-Wagner polarization) (Irimajiri et al., 1987; Ferris et al., 1990; Zhivkov and Gyurova, 2009). In the giga- to terahertz range ($f = 10^9$ – 10^{12} Hz), the relaxation of water and the permittivity difference between cells and electrolytes can cause γ -polarization (Grosse, 2002; Revil et al., 2012).

The relaxation behavior was observed at the frequency from 0.1 to 1 Hz in this study. Therefore, it is presumed to be double-layer polarization or α -polarization, in which the negatively charged surfaces of bacterial cells and the conductive pili, when attached to soil grains, develop double layers and contribute to polarization and thereby increase the imaginary conductivity of the soil (Revil et al., 2012; Zhang et al., 2014; Rosier et al., 2019).

Cole-Cole relaxation modeling of the relaxation response

The accumulation of bacterial cells and biofilms in the sand pack is found to reduce the fluid paths and hence cause a decrease in σ' , particularly at $f > 1$ Hz, primarily due to the reduction in charge passages. However, the double-layer polarization or α -polarization of the accumulated bacterial cells and biofilms is found to cause a significant increase in σ'' with a pronounced relaxation behavior at $f < 100$ Hz. Such a relaxation behavior leads to the σ' difference between low and high frequencies (i.e., $\sigma'_0 - \sigma'_\infty$), which is called normalized chargeability. The observed spectral responses of the complex conductivity associated with the bacterial cells and biofilms in the sand pack are further explored using the Cole-Cole relaxation model, as previously used in the literature (e.g., Revil et al., 2012; Mellage et al., 2018; Rosier et al., 2019).

The Cole-Cole relaxation model was developed by empirical modification of the Debye relaxation model, in which the lower limit of real permittivity at an infinitely high frequency (ϵ'_∞) and the empirical parameter (c), called the Cole-Cole parameter, were introduced (Cole and Cole, 1941). According to the Cole-Cole model, the complex conductivity is described as follows:

$$\sigma'_{\text{eff}} = \sigma'_\infty \left[1 + \frac{M}{2} \left\{ 1 - \frac{\sinh[c \ln(\omega\tau)]}{\cosh[c \ln(\omega\tau)] + \cos\left[\frac{\pi}{2}(1-c)\right]} \right\} \right], \quad (3)$$

and

$$\sigma''_{\text{eff}} = \omega \varepsilon'_{\infty} + \frac{\sigma'_{\infty} M}{2} \cdot \frac{\cos[c \ln(\omega \tau)]}{\cosh[c \ln(\omega \tau)] + \sin\left[\frac{\pi}{2}(1-c)\right]}, \quad (4)$$

where ε'_{∞} is the lower limit value of the real permittivity at high frequency, σ'_{∞} is the lower limit value of the real conductivity at high frequency, c is the Cole-Cole parameter, M is the chargeability, and τ is the relaxation time. Chargeability (M) is defined as the difference between the upper and lower limits of real conductivity divided by the lower limit (i.e., $(\sigma'_0 - \sigma'_{\infty})/\sigma'_{\infty}$), and normalized chargeability (M_n) is defined by multiplying σ'_{∞} by the chargeability; herein, it can be approximated with the measured values at the frequencies of 0.01 Hz and 10 kHz, i.e., $M_n = \sigma'_{[0.01 \text{ Hz}]} - \sigma'_{[10 \text{ kHz}]}$.

The complex conductivity responses measured for the entire column are modeled using the Cole-Cole relaxation model (equations 3 and 4). The complex conductivity obtained at $f = 10^{-1}$ – 10^3 Hz is used to find the best-fit result based on the least-squares method, and the relaxation time (τ) and the Cole-Cole parameter (c) are used as the fitting parameters (Table 3). At high frequency, generally greater than 100 Hz, it is reported that there can be unintended phase error from the measurement system called parasitic capacitive coupling (Wang and Slater, 2019). In this study, we observed significant phase errors at frequencies greater than 1 kHz (Figure 5); therefore, the measured σ^* at $f > 1$ kHz is not used for Cole-Cole modeling. Only σ' values at $f = 10$ kHz are chosen as the lower limit value σ'_{∞} to compute the normalized chargeability. The Cole-Cole model is found to well capture the measured SIP response while our measurement is limited to frequencies of 10^3 Hz.

Figure 9 shows the measured and modeled responses, and it can be seen that the Cole-Cole relaxation model captures the observed complex conductivity responses for the frequency range fairly well over more than four orders of magnitude (i.e., 10^{-1} – 10^3 Hz). The modeled σ' shows remarkably good agreement with the measured σ' for the frequency range from 0.1 to 10^3 Hz, as shown in Figure 9a. Although the Cole-Cole model appears to capture well the imaginary conductivity σ'' at $f > 0.1$ Hz (Figure 9b), it is worth noting that the measured imaginary conductivity σ'' at $f < 0.1$ Hz is much larger than the Cole-Cole model fitting result. This may demonstrate a unique polarization feature of the biomasses produced by the model bacteria *S. oneidensis* MR-1 at $f < 0.1$ Hz. However, the underlying cause of this discrepancy between the Cole-Cole model and the measured trend at very low frequency warrants further research.

Variations in normalized chargeability and relaxation time

The bacterial cell density, cation exchange capacity of the cells, biomass, organic matter, and ion mobility in the pore fluid affect the normalized chargeability (Revil et al., 2012; Zhang et al., 2014; Rosier et al., 2019). A bacterial cell has surface charges that develop a double layer around the cell; therefore, the bacterial cells can be polarized as clay minerals. The microbial organic matter in biofilms and pili produced by *S. oneidensis* MR-1 can have functional groups with highly mobile charges, such that they can serve as charge carriers by attracting and/or transporting

charges (Thormann et al., 2004, 2005; Saville et al., 2011; Roy et al., 2014; Guo et al., 2015). It appears that the normalized chargeability (i.e., $M_n = \sigma'_0 - \sigma'_{\infty}$) increases from 0.004 to 0.11 S/m with time, as shown in Figure 10a. This result is consistent with the hypothesis by Revil et al. (2012) and the experimental observations made by Rosier et al. (2019). The early sharp rise in M_n from 0.004 to approximately 0.07 S/m until 100 h elapsed (approximately 4 days) is mainly attributable to the increase in the biomass in the sand pack, including planktonic cells, attached cells, and biofilms. Because the fresh medium is continuously fed as influent, flushing the planktonic cells, after a certain time the density of the planktonic cells is expected to be maintained rather consistently. Instead, the gradual increase in M_n from approximately 0.07 to 0.11 S/m after 100 h (approximately four days) is presumably caused by the accumulation of biofilms associated with the attached cells.

The relaxation time τ can be estimated by fitting the Cole-Cole model to each SIP response of the whole section, as shown in Figure 10a. The initial relaxation time is approximately 0.9 s at 4 h elapsed, and it decreases to 0.2 s until 100 h elapse (approximately 4 days). Thereafter, the relaxation time converges to approximately 0.16–0.2 s after 100 h. There has been controversy as to whether the accumulation of cells and biofilms would change the relaxation time or not. For instance, it was noted that the relaxation time decreased with an increase in the cell density in the studies by Zhang et al. (2014) and Mellage et al. (2018). On the contrary, Rosier et al. (2019) report that biofilms with bacterial cells and organic material had no or minimal effect on the relaxation time. This study provides clear experimental evidence of a reduction in the relaxation time with microbial activity, which corroborates the observations made by Zhang et al. (2014) and Mellage et al. (2018). It is worth mentioning again that these behaviors are observed in a high-salinity condition, which is different from previous studies.

The relaxation time τ decreases with an increase in the charge mobility (or ion diffusion coefficient) and with reductions in the pore size and polarizable particle size because less time is required to dissipate previous polarization and rearrange charges under a time-varying electric field (Revil et al., 2012; Kruschwitz et al., 2016, 2020). Expectedly, the relaxation characteristics of cells and the organic matter in biofilms differ owing to their different sizes and molecular-scale structures. Different organic components are enveloped in the biofilm EPS, such as lipids, carbohydrates, and

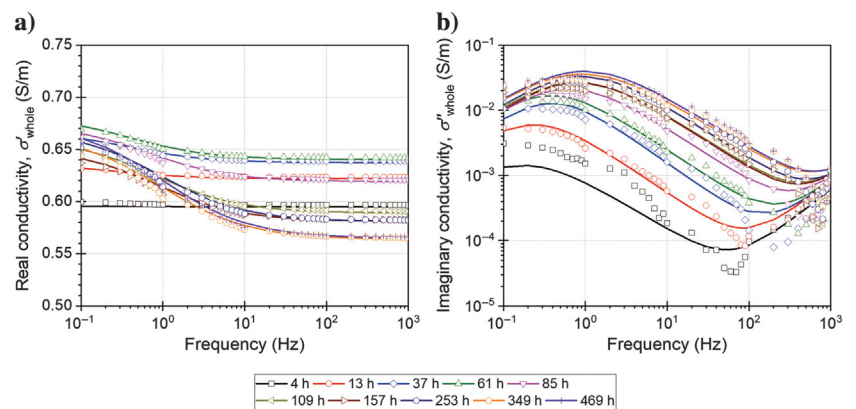


Figure 9. Comparison of the measured values and the Cole-Cole modeling results: (a) real and (b) imaginary conductivity for the whole section. The symbols represent the test results, and the lines indicate the modeling results.

proteins; their sizes are mostly smaller than those of bacterial cells. Therefore, the sharp decrease in τ from 0.9 to 0.2 s in the early days is attributable to a change in the size of polarizable biomasses. In the beginning, the polarizable biomasses are mainly inoculated planktonic bacterial cells. Thereafter, it is presumed that the production of EPS by bacteria causes a decrease in τ , which becomes pronounced after 72 h elapse. After 100 h, the relaxation time stays almost constant, which implies that the microbial system or biomass composition in the sand pack becomes stable; the planktonic/attached cell density and the biofilm composition remain consistent while the EPS accumulates in the sand pack. However, more supporting experiments are warranted under well-controlled conditions to draw a clear conclusion.

It is observed that the normalized chargeability M_n is linearly correlated with the imaginary conductivities σ'' at 1 and 100 Hz, as shown in Figure 10b. Although the slopes are different because our results are associated with the microbial cells and EPS and with high salinity, the linear trend is consistent with the general trends found for the low-salinity conditions in Revil et al. (2017). Furthermore, the relaxation time τ is found to have a power relation with the reciprocal of the imaginary conductivity at 1 Hz $\sigma''_{1\text{ Hz}}$, i.e., $\tau \propto (1/\sigma''_{1\text{ Hz}})^\chi$, where the power exponent χ of 0.64 results in the minimum least-squares error (R^2) for fitting. Moreover, the cell density shows positive relations with $\sigma''_{1\text{ Hz}}$ and M_n , and a negative relation with τ when the cell density is less than 4×10^9 cells/mL, as shown in Figure 10c and 10d. These trends suggest that the SIP and complex conductivity measurement can be an effective way to monitor bacterial growth and bacterial biofilm production in porous media, which is consistent with the previous studies by Abdel Aal et al. (2009), Zhang et al. (2014), and Mellage et al. (2019).

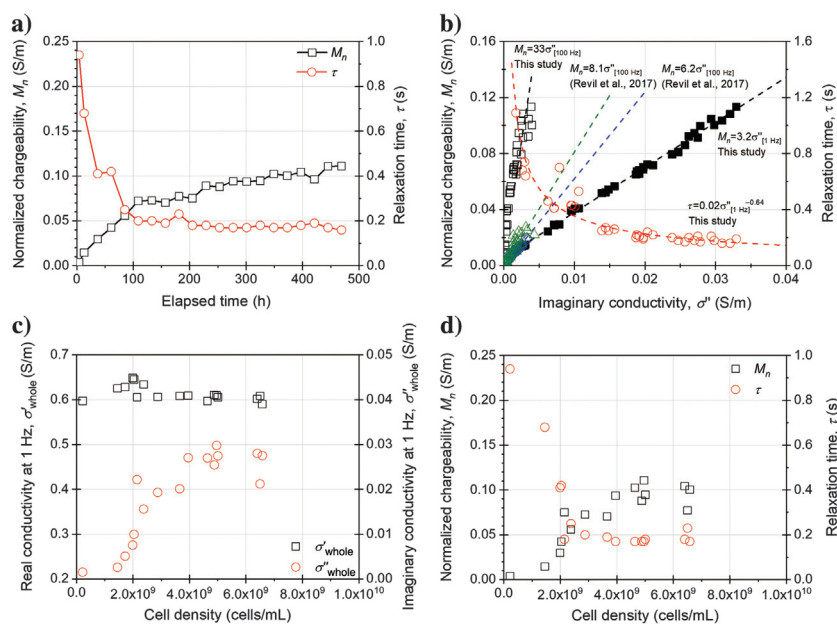


Figure 10. (a) Temporal changes in normalized chargeability and relaxation time for the whole section and (b) the relations between the imaginary conductivity σ'' and normalized chargeability M_n and between the imaginary conductivity σ'' and the relaxation time τ . Additional literature data and trends from Revil et al. (2017) are superimposed for comparison. (c) The complex conductivity σ' and σ'' of the whole section at 1 Hz plotted with the effluent cell density and (d) the normalized chargeability and relaxation time of the whole section plotted with the effluent cell density.

Effect of salinity on normalized chargeability and imaginary conductivity

The normalized chargeability appears to increase from approximately 0.01 S/m to fairly high values of approximately 0.1 S/m. This is possibly associated with our high-salinity condition with pore fluid conductivity σ_w of approximately 2.2–2.4 S/m. It has been previously reported that the normalized chargeability increases with an increase in the pore fluid conductivity and salinity (Gurin et al., 2015; Duvillard et al., 2018). In particular, our normalized chargeability range is in the consistent trend with smectite-rich soils that showed the normalized chargeability of approximately 0.01–0.10 S/m with pore fluid conductivity of approximately 0.1–1.0 S/m (Duvillard et al., 2018). Meanwhile, it is known that the high salinity suppresses the imaginary conductivity and the SIP response (e.g., Kimak et al., 2019). Indeed, Figure 10b shows that, for a given normalized chargeability, the measured imaginary conductivity σ'' at $f = 100$ Hz was much lower than the general trends obtained with σ_w of 0.03 S/m by Revil et al. (2017). Therefore, our results corroborate the previous observations that the high-salinity condition suppresses the IP response, particularly the imaginary conductivity, but it increases the normalized chargeability.

CONCLUSION

This study presents the low-frequency spectral responses of complex conductivity over a frequency range from 10^{-2} to 10^4 Hz during bacterial cell growth of *S. oneidensis* strain and its biofilm formation in a clean nonreactive quartz sand under a highly saline condition with approximately 1% salinity and approximately 2 S/m pore water conductivity. The real conductivity σ' shows two contrasting stages with time: an increase in σ' during the early days, contributed by the metabolites produced by bacteria and the surface conduction of the inoculated bacterial cells, and thereafter a decrease in σ' due to the reduced electron paths by biofilm-induced clogging. However, the imaginary conductivity σ'' shows a significant increase with a pronounced relaxation behavior at $f < 100$ Hz, which is possibly associated with the double-layer polarization of bacterial cells (α -polarization) and the production of electrically conductive EPS and pili. This becomes more distinct with the gradual accumulation of biomass. Fitting the obtained SIP responses to the Cole-Cole model allows examination of variations in the normalized chargeability and the relaxation time. The normalized chargeability increases during cell growth in the early stage, and soon its increasing rate becomes slow during biofilm accumulation in the later stage. Furthermore, the relaxation time rapidly decreases during the early stage; thereafter, it is leveled off, which is presumably attributable to a compositional change in polarizable materials in the pores, mainly from the bacterial cells to the EPS secreted by *S. oneidensis* MR-1. Through comparison with previous literature, it is confirmed that the high-salinity condition increases the normalized chargeability, whereas it suppresses the SIP response and thus

the imaginary conductivity. The presented data suggest the feasibility of using the SIP method to monitor subsurface bacterial activity under high-salinity conditions.

ACKNOWLEDGMENT

The authors are grateful to A. Revil and one anonymous reviewer for their constructive comments and suggestions, which significantly improved the manuscript. This research was supported by the National Research Foundation of Korea (grant no. 2020R1A2C4002358) and by the Nuclear Research and Development Program of the National Research Foundation of Korea (grant no. 2020M2C9A1062949) funded by the Korean government. Y. Wu acknowledges the funding support from U.S. Department of Energy Chemical Sciences, Geosciences, and Biosciences Division under contract no. DE-AC02-05CH11231.

DATA AND MATERIALS AVAILABILITY

Data associated with this research are archived and available in Mendeley Data (<https://data.mendeley.com/>) with the project name “Experimental data of relaxation behavior in low frequency complex conductivity of sands caused by bacterial growth and biofilm formation by *Shewanella oneidensis* under a high salinity condition” (doi: [10.17632/syc95yrykn.5](https://doi.org/10.17632/syc95yrykn.5)). These can also be obtained by contacting the corresponding author. The supporting information provides the bacterial growth kinetics and a calibration curve for the cell density estimation from the optical density (Figure S1), the calibration result of the complex conductivity measurement system developed (Figure S2), the abiotic control test result (Figure S3), and the preliminary test data, which support the repeatability of the experiments (Table S1 and Figure S4). The supplemental information is available online.

REFERENCES

- Abdel Aal, G., E. Atekwana, S. Radzikowski, and S. Rossbach, 2009, Effect of bacterial adsorption on low frequency electrical properties of clean quartz sands and iron-oxide coated sands: *Geophysical Research Letters*, **36**, L04403, doi: [10.1029/2008GL036196](https://doi.org/10.1029/2008GL036196).
- Abdel Aal, G. Z., E. A. Atekwana, and E. A. Atekwana, 2010, Effect of bioclogging in porous media on complex conductivity signatures: *Journal of Geophysical Research*, **115**, G00G07, doi: [10.1029/2009JG001159](https://doi.org/10.1029/2009JG001159).
- Abdel Aal, G. Z., E. A. Atekwana, L. D. Slater, and E. A. Atekwana, 2004, Effects of microbial processes on electrolytic and interfacial electrical properties of unconsolidated sediments: *Geophysical Research Letters*, **31**, L12505, doi: [10.1029/2004GL020030](https://doi.org/10.1029/2004GL020030).
- Abdel-Waly, A. A., 1999, Laboratory study on activating indigenous microorganisms to enhance oil recovery: *Journal of Canadian Petroleum Technology*, **38**, 55–61, doi: [10.2118/99-02-05](https://doi.org/10.2118/99-02-05).
- Amos, R. T., and K. Ulrich Mayer, 2006, Investigating the role of gas bubble formation and entrapment in contaminated aquifers: Reactive transport modelling: *Journal of Contaminant Hydrology*, **87**, 123–154, doi: [10.1016/j.jconhyd.2006.04.008](https://doi.org/10.1016/j.jconhyd.2006.04.008).
- Atekwana, E. A., and L. D. Slater, 2009, Biogeophysics: A new frontier in Earth science research: *Reviews of Geophysics*, **47**, RG4004, doi: [10.1029/2009RG000285](https://doi.org/10.1029/2009RG000285).
- Atekwana, E. A., D. D. Werkema, J. W. Duris, S. Rossbach, E. A. Atekwana, W. A. Sauck, D. P. Cassidy, J. Means, and F. D. Legall, 2004, In-situ apparent conductivity measurements and microbial population distribution at a hydrocarbon-contaminated site: *Geophysics*, **69**, 56–63, doi: [10.1190/1.1649375](https://doi.org/10.1190/1.1649375).
- Cen, L., K. Neoh, and E. Kang, 2004, Antibacterial activity of cloth functionalized with N-alkylated poly (4-vinylpyridine): *Journal of Biomedical Materials Research Part A*, **71**, 70–80.
- Cho, G. C., J. Dodds, and J. C. Santamarina, 2006, Particle shape effects on packing density, stiffness, and strength: Natural and crushed sands: *Journal of Geotechnical and Geoenvironmental Engineering*, **132**, 591–602, doi: [10.1061/\(ASCE\)1090-0241\(2006\)132:5\(591\)](https://doi.org/10.1061/(ASCE)1090-0241(2006)132:5(591)).
- Cole, K. S., and R. H. Cole, 1941, Dispersion and absorption in dielectrics — I: Alternating current characteristics: *The Journal of Chemical Physics*, **9**, 341–351, doi: [10.1063/1.1750906](https://doi.org/10.1063/1.1750906).
- Cortes, D. D., A. I. Martin, T. S. Yun, F. M. Francisca, J. C. Santamarina, and C. Ruppel, 2009, Thermal conductivity of hydrate-bearing sediments: *Journal of Geophysical Research: Solid Earth*, **114**, B11103, doi: [10.1029/2008JB006235](https://doi.org/10.1029/2008JB006235).
- Davis, C. A., E. Atekwana, E. Atekwana, L. D. Slater, S. Rossbach, and M. R. Mormile, 2006, Microbial growth and biofilm formation in geologic media is detected with complex conductivity measurements: *Geophysical Research Letters*, **33**, L18403, doi: [10.1029/2006GL027312](https://doi.org/10.1029/2006GL027312).
- Davis, C. A., L. J. Pyrak-Nolte, E. A. Atekwana, D. D. Werkema, and M. E. Haugen, 2010, Acoustic and electrical property changes due to microbial growth and biofilm formation in porous media: *Journal of Geophysical Research*, **115**, G00G06, doi: [10.1029/2009jg001143](https://doi.org/10.1029/2009jg001143).
- DeJong, J. T., B. M. Mortensen, B. C. Martinez, and D. C. Nelson, 2010, Bio-mediated soil improvement: *Ecological Engineering*, **36**, 197–210, doi: [10.1016/j.ecoleng.2008.12.029](https://doi.org/10.1016/j.ecoleng.2008.12.029).
- Duvillard, P., A. Revil, Y. Qi, A. Soueid Ahmed, A. Coperey, and L. Ravanel, 2018, Three-dimensional electrical conductivity and induced polarization tomography of a rock glacier: *Journal of Geophysical Research: Solid Earth*, **123**, 9528–9554.
- Engel, C., F. Schattenberg, K. Dohnt, U. Schroder, S. Muller, and R. Krull, 2019, Long-term behavior of defined mixed cultures of *Geobacter sulfurreducens* and *Shewanella oneidensis* in bioelectrochemical systems: *Frontiers in Bioengineering and Biotechnology*, **7**, 60, doi: [10.3389/fbioe.2019.00060](https://doi.org/10.3389/fbioe.2019.00060).
- Ferris, L., C. Davey, and D. Kell, 1990, Evidence from its temperature dependence that the β -dielectric dispersion of cell suspensions is not due solely to the charging of a static membrane capacitance: *European Biophysics Journal*, **18**, 267–276, doi: [10.1007/BF00188039](https://doi.org/10.1007/BF00188039).
- Foster, K. R., and H. P. Schwan, 1986, Dielectric properties of tissues: CRC handbook of biological effects of electromagnetic fields: CRC.
- Fröhlich, H., 1975, The extraordinary dielectric properties of biological materials and the action of enzymes: *Proceedings of the National Academy of Sciences*, **72**, 4211–4215.
- Gorby, Y. A., S. Yanina, J. S. McLean, K. M. Rosso, D. Moyles, A. Dohnalkova, T. J. Beveridge, I. S. Chang, B. H. Kim, and K. S. Kim, 2006, Electrically conductive bacterial nanowires produced by *Shewanella oneidensis* strain MR-1 and other microorganisms: *Proceedings of the National Academy of Sciences*, **103**, 11358–11363, doi: [10.1073/pnas.0604517103](https://doi.org/10.1073/pnas.0604517103).
- Grosse, C., 2002, Relaxation mechanisms of homogeneous particles and cells suspended in aqueous electrolyte solutions: *Interfacial Electrokinetics and Electrophoresis*, **106**, 279–327.
- Guo, W., S. Luo, Z. He, and X. Feng, 2015, 13C pathway analysis of biofilm metabolism of *Shewanella oneidensis* MR-1: *Royal Society of Chemistry Advances*, **5**, 39840–39843, doi: [10.1039/c5ra05573c](https://doi.org/10.1039/c5ra05573c).
- Gurin, G., K. Titov, Y. Ilyin, and A. Tarasov, 2015, Induced polarization of disseminated electronically conductive minerals: A semi-empirical model: *Geophysical Journal International*, **200**, 1555–1565, doi: [10.1093/gji/ggu490](https://doi.org/10.1093/gji/ggu490).
- Ham, S. M., I. Chang, D. H. Noh, T.-H. Kwon, and B. Muhunthan, 2018, Improvement of surface erosion resistance of sand by microbial biopolymer formation: *Journal of Geotechnical and Geoenvironmental Engineering*, **144**, 06018004, doi: [10.1061/\(ASCE\)GT.1943-5606.0001900](https://doi.org/10.1061/(ASCE)GT.1943-5606.0001900).
- Icopini, G. A., J. G. Lack, L. E. Hersman, M. P. Neu, and H. Boukhalfa, 2009, Plutonium(V/VI) reduction by the metal-reducing bacteria *Geobacter metallireducens* GS-15 and *Shewanella oneidensis* MR-1: *Applied and Environmental Microbiology*, **75**, 3641–3647, doi: [10.1128/AEM.00022-09](https://doi.org/10.1128/AEM.00022-09).
- Irimajiri, A., K. Asami, T. Ichinowatari, and Y. Kinoshita, 1987, Passive electrical properties of the membrane and cytoplasm of cultured rat basophil leukemia cells — I: Dielectric behavior of cell suspensions in 0.01–500 MHz and its simulation with a single-shell model: *Biochimica et Biophysica Acta (BBA)-Biomembranes*, **896**, 203–213, doi: [10.1016/0005-2736\(87\)90181-7](https://doi.org/10.1016/0005-2736(87)90181-7).
- Karaoulis, M., A. Revil, D. Werkema, B. Minsley, W. Woodruff, and A. Kenna, 2011, Time-lapse three-dimensional inversion of complex conductivity data using an active time constrained (ATC) approach: *Geophysical Journal International*, **187**, 237–251, doi: [10.1111/j.1365-246X.2011.05156.x](https://doi.org/10.1111/j.1365-246X.2011.05156.x).
- Kim, Y. M., T. Park, and T. H. Kwon, 2019, Engineered bioclogging in coarse sands by using fermentation-based bacterial biopolymer formation: *Geomechanics and Engineering*, **17**, 485–496, doi: [10.12989/gae.2019.17.5.485](https://doi.org/10.12989/gae.2019.17.5.485).
- Kimak, C., D. Ntarlagiannis, L. Slater, E. Atekwana, C. Beaver, S. Rossbach, A. Porter, and A. Ustra, 2019, Geophysical monitoring of hydrocarbon biodegradation in highly conductive environments: *Journal of Geophysical Research: Biogeosciences*, **124**, 353–366.
- Kruschwitz, S., M. Halisch, R. Dlugosch, and C. Prinz, 2020, Toward a better understanding of low-frequency electrical relaxation — An enhanced pore space characterization: *Geophysics*, **85**, no. 4, MR257–MR270, doi: [10.1190/geo2019-0074.1](https://doi.org/10.1190/geo2019-0074.1).

- Kruschwitz, S., C. Prinz, and A. Zimathies, 2016, Study into the correlation of dominant pore throat size and SIP relaxation frequency: *Journal of Applied Geophysics*, **135**, 375–386, doi: [10.1016/j.jappgeo.2016.07.007](https://doi.org/10.1016/j.jappgeo.2016.07.007).
- Kwon, T. H., and J. B. Ajo-Franklin, 2013, High-frequency seismic response during permeability reduction due to biopolymer clogging in unconsolidated porous media: *Geophysics*, **78**, no. 6, EN117–EN127, doi: [10.1190/geo2012-0392.1](https://doi.org/10.1190/geo2012-0392.1).
- Lee, S., D. H. Kim, and K. W. Kim, 2018, The enhancement and inhibition of mercury reduction by natural organic matter in the presence of *Shewanella oneidensis* MR-1: *Chemosphere*, **194**, 515–522, doi: [10.1016/j.chemosphere.2017.12.007](https://doi.org/10.1016/j.chemosphere.2017.12.007).
- Mellage, A., C. M. Smeaton, A. Furman, E. A. Atekwana, F. Rezanezhad, and P. Van Cappellen, 2018, Linking spectral induced polarization (SIP) and subsurface microbial processes: Results from sand column incubation experiments: *Environmental Science & Technology*, **52**, 2081–2090, doi: [10.1021/acs.est.7b04420](https://doi.org/10.1021/acs.est.7b04420).
- Mellage, A., C. M. Smeaton, A. Furman, E. A. Atekwana, F. Rezanezhad, and P. Van Cappellen, 2019, Bacterial Stern layer diffusion: Experimental determination with spectral induced polarization and sensitivity to nitrite toxicity: *Near Surface Geophysics*, **17**, 623–635, doi: [10.1002/nsg.12058](https://doi.org/10.1002/nsg.12058).
- Mitchell, J. K., and J. C. Santamarina, 2005, Biological considerations in geotechnical engineering: *Journal of Geotechnical and Geoenvironmental Engineering*, **131**, 1222–1233, doi: [10.1061/\(ASCE\)1090-0241\(2005\)131:10\(1222\)](https://doi.org/10.1061/(ASCE)1090-0241(2005)131:10(1222)).
- Noh, D. H., J. B. Ajo-Franklin, T. H. Kwon, and B. Muhunthan, 2016, P and S wave responses of bacterial biopolymer formation in unconsolidated porous media: *Journal of Geophysical Research: Biogeosciences*, **121**, 1158–1177, doi: [10.1002/2015jg003118](https://doi.org/10.1002/2015jg003118).
- Ntarlagiannis, D., and A. Ferguson, 2009, SIP response of artificial biofilms: *Geophysics*, **74**, no. 1, A1–A5, doi: [10.1190/1.3031514](https://doi.org/10.1190/1.3031514).
- Ntarlagiannis, D., N. Yee, and L. Slater, 2005, On the low-frequency electrical polarization of bacterial cells in sands: *Geophysical Research Letters*, **32**, 2–5, doi: [10.1029/2005GL024751](https://doi.org/10.1029/2005GL024751).
- Park, T., H. W. Joo, G. Y. Kim, S. Kim, S. Yoon, and T. H. Kwon, 2017, Biosurfactant as an enhancer of geologic carbon storage: Microbial modification of interfacial tension and contact angle in carbon dioxide/water/quartz systems: *Frontiers in Microbiology*, **8**, 1285, doi: [10.3389/fmicb.2017.01285](https://doi.org/10.3389/fmicb.2017.01285).
- Revil, A., E. Atekwana, C. Zhang, A. Jardani, and S. Smith, 2012, A new model for the spectral induced polarization signature of bacterial growth in porous media: *Water Resources Research*, **48**, W09545, doi: [10.1029/2012WR011965](https://doi.org/10.1029/2012WR011965).
- Revil, A., A. Coperey, Z. Shao, N. Florsch, I. L. Fabricius, Y. Deng, J. Delsman, P. Pauw, M. Karoulis, and P. de Louw, 2017, Complex conductivity of soils: *Water Resources Research*, **53**, 7121–7147, doi: [10.1002/2017WR020655](https://doi.org/10.1002/2017WR020655).
- Revil, A., and M. Skold, 2011, Salinity dependence of spectral induced polarization in sands and sandstones: *Geophysical Journal International*, **187**, 813–824, doi: [10.1111/j.1365-246X.2011.05181.x](https://doi.org/10.1111/j.1365-246X.2011.05181.x).
- Rosier, C. L., E. A. Atekwana, G. A. Aal, and M. A. Patrauchan, 2019, Cell concentrations and metabolites enhance the SIP response to biofilm matrix components: *Journal of Applied Geophysics*, **160**, 183–194, doi: [10.1016/j.jappgeo.2018.10.023](https://doi.org/10.1016/j.jappgeo.2018.10.023).
- Roy, J. N., S. Babanova, K. E. Garcia, J. Cornejo, L. K. Ista, and P. Atanassov, 2014, Catalytic biofilm formation by *Shewanella oneidensis* MR-1 and anode characterization by expanded uncertainty: *Electrochimica Acta*, **126**, 3–10, doi: [10.1016/j.electacta.2013.07.075](https://doi.org/10.1016/j.electacta.2013.07.075).
- Roy, J. N., K. E. Garcia, H. R. Luckarift, A. Falase, J. Cornejo, S. Babanova, A. J. Schuler, G. R. Johnson, and P. B. Atanassov, 2013, Applied electrode potential leads to *Shewanella oneidensis* MR-1 biofilms engaged in direct electron transfer: *Journal of the Electrochemical Society*, **160**, H866–H871, doi: [10.1149/2.001401jes](https://doi.org/10.1149/2.001401jes).
- Saville, R. M., S. Rakshe, J. A. Haagensen, S. Shukla, and A. M. Spormann, 2011, Energy-dependent stability of *Shewanella oneidensis* MR-1 biofilms: *Journal of Bacteriology*, **193**, 3257–3264, doi: [10.1128/JB.00251-11](https://doi.org/10.1128/JB.00251-11).
- Slater, L. D., J. Choi, and Y. X. Wu, 2005, Electrical properties of iron-sand columns: Implications for induced polarization investigation and performance monitoring of iron-wall barriers: *Geophysics*, **70**, no. 4, G87–G94, doi: [10.1190/1.1990218](https://doi.org/10.1190/1.1990218).
- Thormann, K. M., R. M. Saville, S. Shukla, D. A. Pelletier, and A. M. Spormann, 2004, Initial phases of biofilm formation in *Shewanella oneidensis* MR-1: *Journal of Bacteriology*, **186**, 8096–8104, doi: [10.1128/JB.186.23.8096-8104.2004](https://doi.org/10.1128/JB.186.23.8096-8104.2004).
- Thormann, K. M., R. M. Saville, S. Shukla, and A. M. Spormann, 2005, Induction of rapid detachment in *Shewanella oneidensis* MR-1 biofilms: *Journal of Bacteriology*, **187**, 1014–1021, doi: [10.1128/JB.187.3.1014-1021.2005](https://doi.org/10.1128/JB.187.3.1014-1021.2005).
- Ulrich, C., and L. Slater, 2004, Induced polarization measurements on unsaturated, unconsolidated sands: *Geophysics*, **69**, 762–771, doi: [10.1190/1.1759462](https://doi.org/10.1190/1.1759462).
- Wang, C., and L. D. Slater, 2019, Extending accurate spectral induced polarization measurements into the kHz range: Modelling and removal of errors from interactions between the parasitic capacitive coupling and the sample holder: *Geophysical Journal International*, **218**, 895–912, doi: [10.1093/gji/ggz199](https://doi.org/10.1093/gji/ggz199).
- Weller, A., Z. Zhang, and L. Slater, 2015, High-salinity polarization of sandstones: *Geophysics*, **80**, no. 3, D309–D318, doi: [10.1190/geo2014-0483.1](https://doi.org/10.1190/geo2014-0483.1).
- Williams, K. H., D. Ntarlagiannis, L. D. Slater, A. Dohnalkova, S. S. Hubbard, and J. F. Banfield, 2005, Geophysical imaging of stimulated microbial biomineralization: *Environmental Science & Technology*, **39**, 7592–7600, doi: [10.1021/es0504035](https://doi.org/10.1021/es0504035).
- Wu, Y., and L. Peruzzo, 2020, Effects of salinity and pH on the spectral induced polarization signals of graphite particles: *Geophysical Journal International*, **221**, 1532–1541, doi: [10.1093/gji/ggaa087](https://doi.org/10.1093/gji/ggaa087).
- Wu, Y. X., V. K. Surasani, L. Li, and S. S. Hubbard, 2014, Geophysical monitoring and reactive transport simulations of bioclogging processes induced by *Leuconostoc mesenteroides*: *Geophysics*, **79**, no. 1, E61–E73, doi: [10.1190/geo2013-0121.1](https://doi.org/10.1190/geo2013-0121.1).
- Xiong, Y. J., L. Shi, B. W. Chen, M. U. Mayer, B. H. Lower, Y. Londer, S. Bose, M. F. Hochella, J. K. Fredrickson, and T. C. Squier, 2006, High-affinity binding and direct electron transfer to solid metals by the *Shewanella oneidensis* MR-1 outer membrane c-type cytochrome OmcA: *Journal of the American Chemical Society*, **128**, 13978–13979, doi: [10.1021/ja063526d](https://doi.org/10.1021/ja063526d).
- Zhang, C., A. Revil, Y. Fujita, J. Munakata-Marr, and G. Redden, 2014, Quadrature conductivity: A quantitative indicator of bacterial abundance in porous media: *Geophysics*, **79**, no. 6, D363–D375, doi: [10.1190/geo2014-0107.1](https://doi.org/10.1190/geo2014-0107.1).
- Zhang, C., L. Slater, and C. Prodan, 2013, Complex dielectric properties of sulfate-reducing bacteria suspensions: *Geomicrobiology Journal*, **30**, 490–496, doi: [10.1080/01490451.2012.719997](https://doi.org/10.1080/01490451.2012.719997).
- Zhang, T. C., Y. C. Fu, P. L. Bishop, M. Kupferle, S. Fitzgerald, H. H. Jiang, and C. Harmer, 1995, Transport and biodegradation of toxic organics in biofilms: *Journal of Hazardous Materials*, **41**, 267–285, doi: [10.1016/0304-3894\(94\)00118-Z](https://doi.org/10.1016/0304-3894(94)00118-Z).
- Zhivkov, A. M., and A. Y. Gyurova, 2009, Influence of cytoplasm electrolyte concentration on Maxwell-Wagner polarizability of bacteria *E. coli*: *The Journal of Physical Chemistry B*, **113**, 8375–8382, doi: [10.1021/jp810020p](https://doi.org/10.1021/jp810020p).
- Zimmermann, E., A. Kemna, J. Berwix, W. Glaas, H. M. Münch, and J. A. Huisman, 2008, A high-accuracy impedance spectrometer for measuring sediments with low polarizability: *Measurement Science and Technology*, **19**, 105603, doi: [10.1088/0957-0233/19/10/105603](https://doi.org/10.1088/0957-0233/19/10/105603).

Biographies and photographs of the authors are not available.